FULL PAPER　　　　　　　　　　　　　　　　　　**Open Access**

Fault weakening caused by smectite swelling

Jun Kameda[1*] , Masaoki Uno[2], Marianne Conin[3], Kohtaro Ujiie[4], Yohei Hamada[5] and Gaku Kimura[6]

Abstract

The large slip along the shallow subduction interface during the 2011 Tohoku-Oki earthquake ($M_w9.0$) caused a huge tsunami that struck the northeast coast of Honshu, Japan. The Integrated Ocean Drilling Program Expedition 343 JFAST program revealed that the fault zone is composed primarily of smectite. Our swelling experiments using the fault material demonstrated that the swelling pressure systematically increases with a decrease in sample porosity. Based on in situ porosity estimations in the IODP borehole, the swelling pressure of the fault is as high as 8 MPa, which is comparable to the effective normal stress at the drill site (~ 7 MPa). This also suggests that the modified effective confining pressure of the fault is quite low or potentially zero, meaning that fault strength is governed mainly by cohesion rather than frictional strength. The fault may therefore be intrinsically weak, which could enhance the coseismic displacement toward the trench when earthquake slip propagates from depth.

Keywords: 2011 Tohoku-Oki earthquake, Fault strength, Smectite, Swelling

Introduction

Smectite, which is a common clay mineral in the shallow crust, swells when in contact with water (Mitchell and Soga 2005). The immersion of smectite-containing rocks, such as bentonite, causes expansion, and a swelling pressure develops if the volume is restricted. Experiments with compacted bentonites have shown swelling pressures of several tens of MPa (e.g., Tripathy et al. 2004). Such swelling and accompanying pressure can deform soils and foundations, posing a threat to human activities (Mitchell and Soga 2005).

Smectite is also a typical component of shallow crustal faults (Vrolijk and van der Pluijm 1999), and numerous studies have examined the frictional properties of smectite and its relationship to earthquakes (Logan and Rauenzahn 1987; Moore and Lockner 2007; Saffer et al. 2001). In addition to its intrinsic low friction, smectite swelling pressure can influence the stress state of the solid matrix within the fault. The effective stress acting on a fault (σ_n') is generally described as

$$\sigma_n' = \sigma_n - P_f, \tag{1}$$

where σ_n is the normal stress and P_f is the fluid pressure. If the fault zone is composed primarily of swelling clays, the swelling pressure (P_s) needs to be taken into account by considering a modified effective confining pressure (σ_n''; Chatterji and Morgenstern 1990), where

$$\sigma_n'' = \sigma_n' - P_s. \tag{2}$$

A modified shear strength formulation, following the Coulomb failure criterion, has been validated from shearing tests of montmorillonite soils (Chatterji and Morgenstern 1990) as follows:

$$\tau_{res} = c' + \sigma_n'' \tan \varphi_{res}, \tag{3}$$

where τ_{res} is the residual shear strength, c' is the residual effective cohesion and φ_{res} is the residual friction angle. Therefore, the influence of smectite swelling pressure on the stress state of the fault is similar to that of pore fluid pressure. Experiments have also shown that the effective stress plays a fundamental role in the slip behaviour of smectite gouges (Ikari et al. 2007; Moore and Lockner 2007). However, few studies have focused on the swelling behaviour of smectite in fault zones (Deng and Underwood 2001; Kameda et al. 2010), and none of these has

*Correspondence: kameda@sci.hokudai.ac.jp
[1] Department of Earth and Planetary Sciences, Graduate School of Science, Hokkaido University, N10 W8, Sapporo 060-0810, Japan
Full list of author information is available at the end of the article

addressed its potential relevance to earthquake mechanics. Here we provide the first documentation of a possible link between smectite swelling in an active fault and the generation of a large earthquake.

2011 Tohoku-Oki earthquake (Mw9.0) and the source fault

The 11 March 2011 Mw9.0 Tohoku-Oki earthquake was the largest event in Japan's long recorded seismic history. The coseismic rupture and slip of the earthquake propagated to the trench along the plate boundary fault (Ide et al. 2011; Fujii et al. 2011; Fujiwara et al. 2011; Kodaira et al. 2012), generating a huge tsunami that resulted in massive damage along the northeast coast of Honshu. The shallow part of the plate interface has generally been considered as a zone of stable slip, meaning that the propagation of slip and rupture to such shallow crustal depths was unexpected.
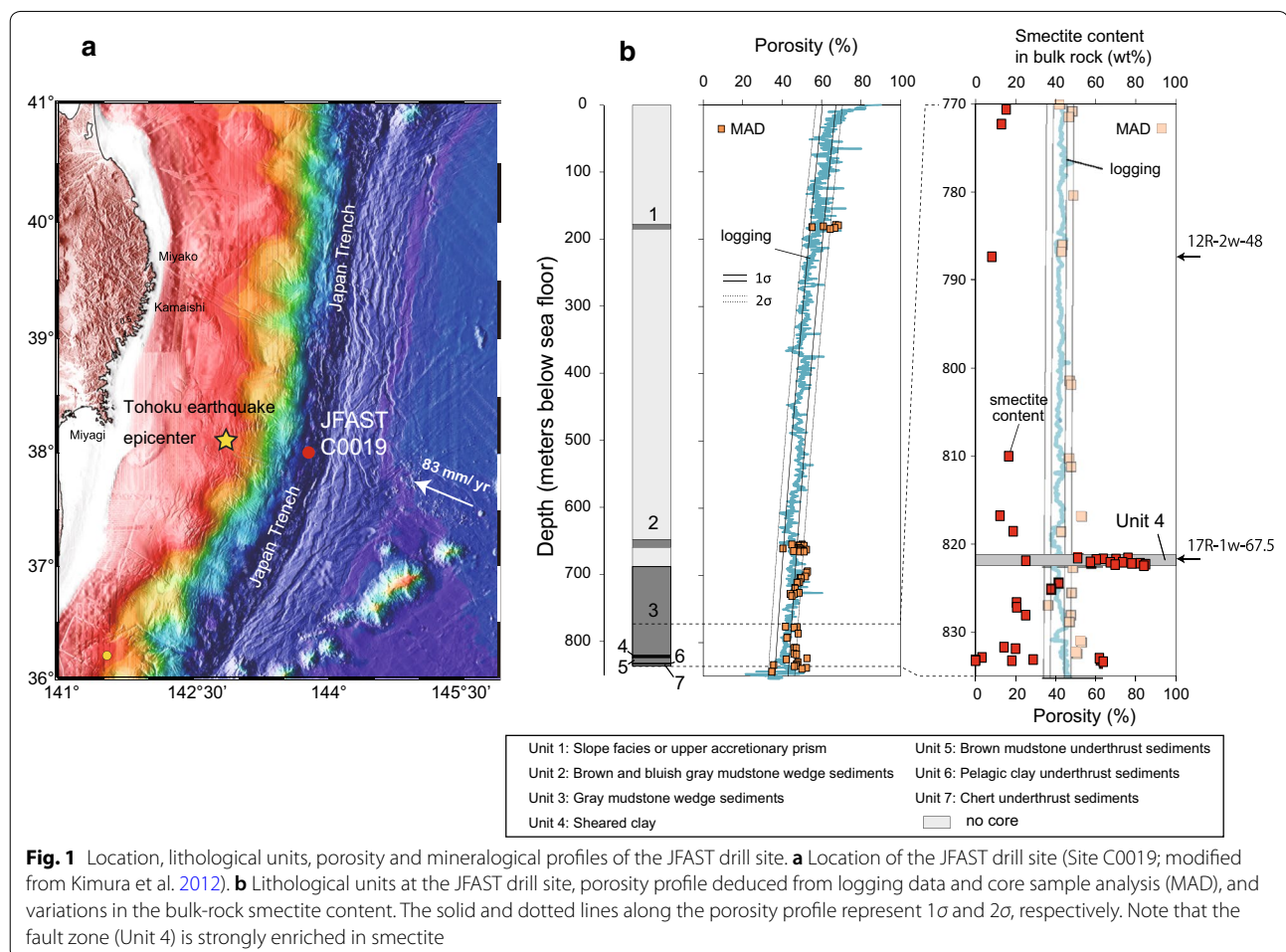
One year after the Tohoku-Oki earthquake, deep-sea drilling by the Integrated Ocean Drilling Program (IODP Expedition 343 JFAST program) was carried out to directly investigate the shallow source fault of the earthquake (Chester et al. 2012, 2013). The drilling at site C0019E, 5 km landward from the trench axis where the largest fault slip (> 50 m) occurred (Fig. 1a), identified a < 5-m-thick plate boundary fault zone at ~ 820 m below the sea floor (mbsf; Fig. 1b; Chester et al. 2013) and recovered core samples of the fault zone. Mineralogical analyses of the core samples revealed that the fault zone is marked by an extremely high concentration of smectite (60–80 wt%) as compared with surrounding sequences (< 20 wt%; Fig. 1b; Kameda et al. 2015).

Experimental
Swelling experiments

We conducted laboratory swelling experiments using the powdered core samples recovered from the borehole to estimate the in situ swelling pressures of the Tohoku fault zone. A sample from the host rock (12R-2w-48–52 cm; grey mudstone interval) and another from the fault zone (17R-1w-67.5–69 cm) were tested using the apparatus shown in Fig. 2a. Figure 1b shows the locations of these
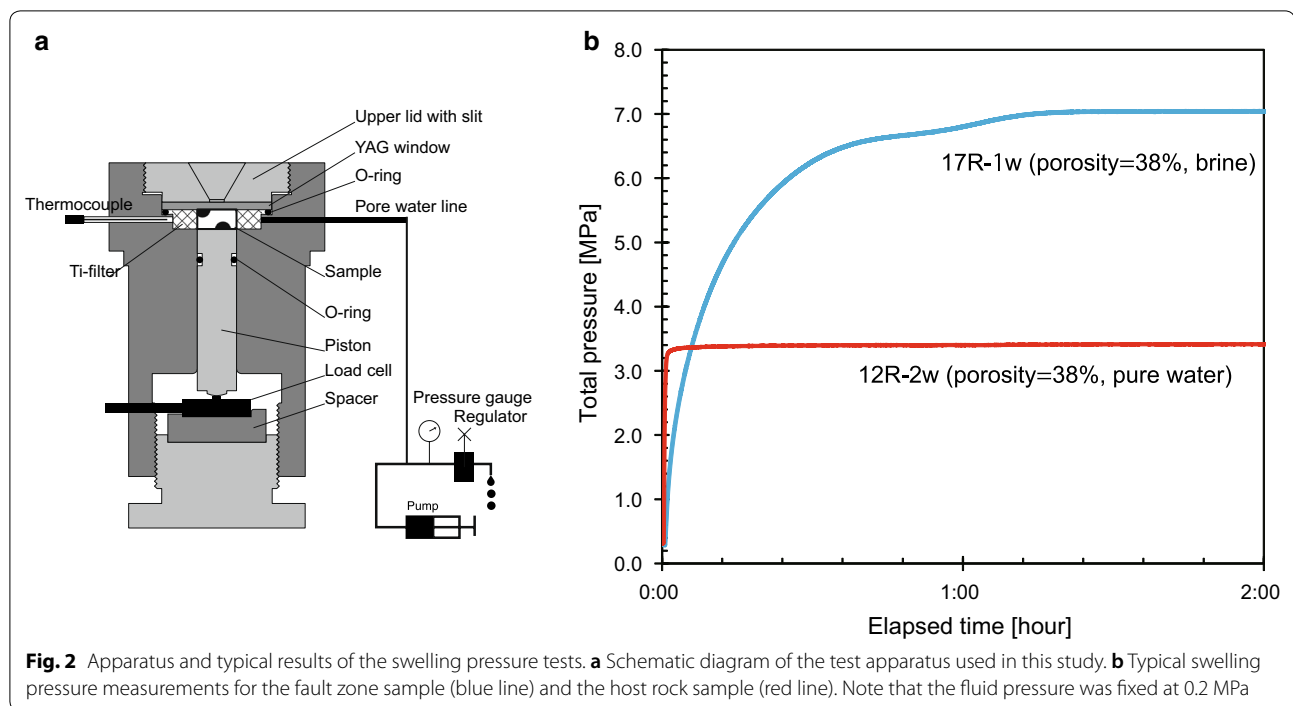

Fig. 1 Location, lithological units, porosity and mineralogical profiles of the JFAST drill site. **a** Location of the JFAST drill site (Site C0019; modified from Kimura et al. 2012). **b** Lithological units at the JFAST drill site, porosity profile deduced from logging data and core sample analysis (MAD), and variations in the bulk-rock smectite content. The solid and dotted lines along the porosity profile represent 1σ and 2σ, respectively. Note that the fault zone (Unit 4) is strongly enriched in smectite

Fig. 2 Apparatus and typical results of the swelling pressure tests. **a** Schematic diagram of the test apparatus used in this study. **b** Typical swelling pressure measurements for the fault zone sample (blue line) and the host rock sample (red line). Note that the fluid pressure was fixed at 0.2 MPa

two samples in relation to the fault zone (fundamental properties of the samples are also shown in Additional file 1: Table S1). The swelling pressure of the expanding rock has been previously estimated using Gouy–Chapman theory, which is based on the repulsive force that stems from an overlap of the diffuse double-layers of adjacent charged plates (i.e., diffuse double-layer theory; Bolt 1955; van Olphen 1963; Mitchell and Soga 2005). However, the salinity of fault zone pore fluid is as high as that of seawater (Kameda et al. 2016), indicating that this theory cannot precisely predict reasonable pressure values (Komine et al. 2009). Therefore, we used both pure water and artificial pore water ($Na^+ = 455.8$ mM; $Ca^{2+} = 24.7$ mM; $K^+ = 7.7$ mM; $Mg^{2+} = 37.8$ mM; Kameda et al. 2016) as the reacting fluids at a fluid pressure of 0.2 MPa. We only measured the pressures under pure water conditions for the host rock sample (12R-2w-48–52 cm). A previous experiment demonstrated that the swelling pressures in brine are equal to or smaller than those in pure water (Komine et al. 2009), indicating that data for the host rock represent the upper bound of the system.

The swelling tests were performed using 0.3 g of the ground powders (except for Test 05; Additional file 1: Table S1), stored and weighed at room humidity, employing a cylindrical sample cell ($\Phi = 0.8$ mm) in the apparatus (Fig. 2a). We did not heat the powders to obtain the dried samples, because such treatment could potentially damage their swelling properties (Schleicher et al.

2015). The samples were pre-compacted to the objective porosity (see Additional file 1 for estimation of sample porosity), and the piston position was fixed to avoid a volumetric expansion of the wet sample, thereby maintaining the sample porosity during the test.

Porosity estimates from borehole logging data

Our porosity estimates refer to the 'total porosity' (Conin et al. 2011), which is defined by the total volume of water in intergranular pore spaces and the mineral assemblage, as well as what is adsorbed at the mineral surface. We estimated the downhole porosity (ϕ) from the resistivity logging data using Archie's law:

$$\phi = \left(a \times \frac{\sigma_b}{\sigma_f} \right)^{\frac{1}{m}}, \tag{4}$$

where the constant a is equal to one (see Conin et al. 2011 for an explanation). The parameter m was determined by fitting the porosity estimations from logs to the core measurements (Chester et al. 2012), using a least-squares method. In this case, $m = 2.7$. The porosity of the cores was obtained from MAD (moisture and density) measurements (Blum 1997). The bulk conductivity of the sediments (σ_b) was measured from the resistivity logging data (Chester et al. 2012). The interstitial fluid conductivity (σ_f) was computed from the downhole temperature (T, in °C; Bourlange et al. 2003) as

Kameda *et al. Earth, Planets and Space*   (2019) 71:131

Page 4 of 7

$$\sigma_f = 5.32 \times \{1 + 0.02 \times (T - 25)\}. \tag{5}$$

The downhole temperature was calculated as

$$T = \frac{HF}{TC} \times Z + T_0, \tag{6}$$

where TC is the thermal conductivity (1.1 W m^{-1} K^{-1}; Chester et al. 2012), HF is the heat flow (45 mW m^{-2}; Tanaka et al. 2004; Yamano et al. 2008; Gao and Wang 2014), T_0 is the measured surface temperature (1.3 °C) and Z is depth below the seafloor (m).

Results

The porosity change along the borehole was estimated from the logging data, as well as onboard measurements of the recovered samples (Fig. 1b; Chester et al. 2012), showing a compaction trend from 60 to 80% porosity just below the seafloor to 36–40% within the fault zone. Slightly higher porosities from in recovered cores (MAD measurements in Fig. 1b) are attributed to core rebound due to the release of confining pressure.

Figure 2b shows an example of the swelling pressure test. The host rock sample exhibited a rapid increase in swelling pressure within the first ~2 min of the test to the maximum value (3.3 MPa), and this pressure was maintained until the end of the test (70 h). However, the fault zone sample exhibited a more gradual increase in pressure to the maximum value (7 MPa) after ~8 h, and this pressure was maintained until the end of the test (17 h). Given the fluid pressure of 0.2 MPa, the excess pressure is taken as the swelling pressure. Figure 3 shows the observed swelling pressures of the fault zone (blue) and the host rock samples (red) as a function of sample porosity (Table 1). For both samples, the swelling pressure increases with decreasing porosity, resulting in closer distances between the repulsive clay particles (Fig. 3). The results also indicate that the swelling pressure becomes higher in the fault zone than in the host rock intervals at a given porosity, reflecting the higher abundance of smectite in the fault zone (Fig. 1).

Discussion and conclusions

Our swelling experiments demonstrate that the swelling pressure of each sample systematically increases with decrease of porosity. According to Hedin (2004), the relationship between the swelling pressure P_s (MPa) and water-saturated clay density ρ_c can be expressed empirically as follows:

$$P_s = A \times T \left\{ \exp\left\{ B \frac{\rho_s(\rho_c - \rho_f)}{\rho_f(\rho_s - \rho_c)} \right\} - 1 \right\} \times \frac{1}{1000}, \tag{7}$$
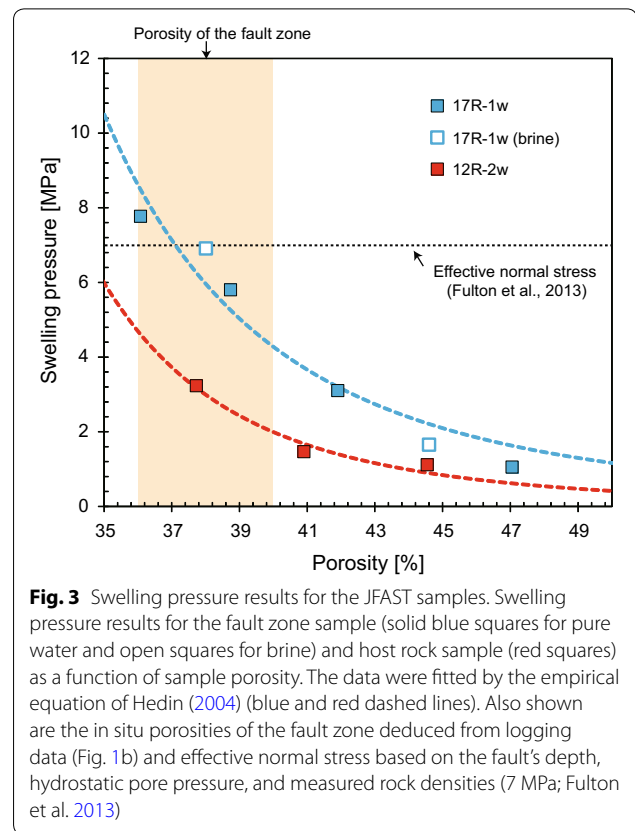

Fig. 3 Swelling pressure results for the JFAST samples. Swelling pressure results for the fault zone sample (solid blue squares for pure water and open squares for brine) and host rock sample (red squares) as a function of sample porosity. The data were fitted by the empirical equation of Hedin (2004) (blue and red dashed lines). Also shown are the in situ porosities of the fault zone deduced from logging data (Fig. 1b) and effective normal stress based on the fault's depth, hydrostatic pore pressure, and measured rock densities (7 MPa; Fulton et al. 2013)

where A and B are fitting parameters, T is the temperature (K) and ρ_f and ρ_s are the densities of water (1.0 g/cm^3) and solid particles, respectively. According to Conin et al. (2014), ρ_c is related to ρ_s through the sample porosity ϕ as

$$\rho_c = \rho_s + \phi(\rho_f - \rho_s). \tag{8}$$

The fault zone and host rock data of the present study are consistent with Eq. (7), with fitting parameters of $A = 0.36$ and $B = 0.87$, and $A = 0.068$ and $B = 1.17$, respectively (dashed lines in Fig. 3). The fault zone data for pure and brine waters are represented by a single best-fit curve.

Comparison of the experimental results with the borehole porosity profile indicates that the swelling pressure is as high as ~8 MPa within the fault zone (Fig. 3), which is 0.6–1.2 times the effective normal stress $\sigma_n{}'$ applied on the fault based on the fault's depth, hydrostatic pore pressure, and measured rock densities (~7 MPa; Fulton et al. 2013). Considering Eqs. (2) and (3), this suggests that the modified effective confining pressure $\sigma_n{}''$, and thus the frictional strength, of the fault is quite low or potentially zero, meaning that cohesion c' is the dominant component of the shear strength of the fault.

Kameda *et al. Earth, Planets and Space*   (2019) 71:131

Page 5 of 7

Table 1 Summary of the experiments

Test	Sample	Solution	Weight (g)	ρ_r (g/cm^3)[a]	Porosity (%)	Temperature (°C)	Fluid pressure (MPa)	Total pressure (MPa)[b]	Swelling pressure (MPa)[b]	Time to maximum pressure (h)
00	17R-1W	DW	0.300	1.98	47.5	Ambient	0.2	1.25	1.05	10.84
01	17R-1W	DW	0.300	2.08	42.0	Ambient	0.2	3.30	3.10	24.78
02	17R-1W	DW	0.300	2.19	36.0	Ambient	0.2	7.97	7.77	17.46
03	17R-1W	DW	0.300	2.14	38.7	20	0.2	6.03	5.83	21.31
04	12R-2W	DW	0.300	2.01	37.7	25	0.2	3.43	3.23	7.29
05	12R-2W	DW	0.284	1.96	40.9	26.5–21.6	0.2	1.66	1.46	1.57
06	12R-2W	DW	0.300	1.90	44.7	25	0.2	1.31	1.11	0.03
07	17R-1W	Brine	0.300	2.15	38.0	25	0.2	7.11	6.91	7.72
08	17R-1W	Brine	0.300	2.03	44.6	25	0.2	1.85	1.65	6.47

DW distilled water

[a] Water-saturated sample density

[b] Values represent the maximum pressures

Figure 4 shows how the swelling pressure of the fault changes at depths estimated from extrapolation of the porosity and swelling pressure curves. The effective normal stress at depths is also estimated from the porosity curve and the representative rock density of the recovered cores (2.6 g/cm^3). Although the effective normal stress increases with depth, the swelling pressure increases more rapidly, implying that effective normal stress applied on the fault can be fully supported by the swelling pressure. Because of a low thermal structure of the Japan Trench, smectite–illite transition is suppressed within 100 km distant from the trench (Kimura et al. 2012; Kameda et al. 2012), suggesting that the swelling of smectite may have a potential to weaken the wide area of the shallow plate interface. It should be noted, however, that when the temperature increases with depth, the swelling ability of clays may be reduced due to dissolution and collapse of smectite particles (Tessier et al. 1998; Schleicher et al. 2015). In addition, when the effective normal stress increases with depth, the interlayer water can be removed from the interlayer space, resulting in the deswelling. The driving forces of swelling would be the free-energy difference among bulk water, interlayer water, and clay. The energy balance may depend on the effective normal stress and temperature. Therefore, the extrapolated swelling behaviors shown in Fig. 4 should be verified by future experiments.

Although the estimated porosity represents the postseismic state of the fault, we infer that the porosity before the earthquake was no higher than that after the earthquake, because the coseismic slip zone often exhibits a decrease in density relative to the surrounding rocks after
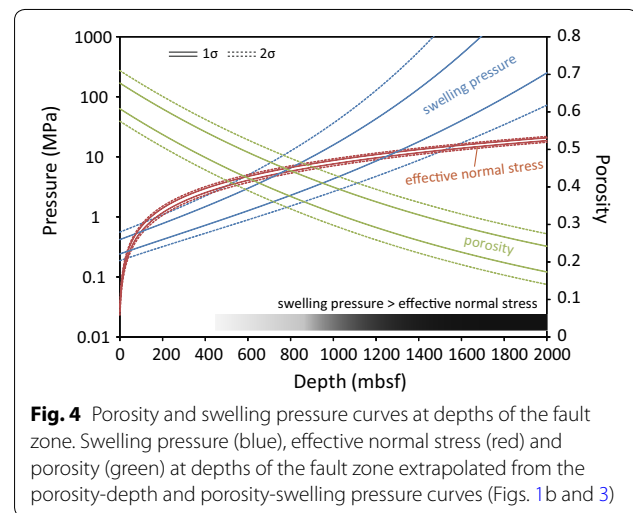

Fig. 4 Porosity and swelling pressure curves at depths of the fault zone. Swelling pressure (blue), effective normal stress (red) and porosity (green) at depths of the fault zone extrapolated from the porosity-depth and porosity-swelling pressure curves (Figs. 1b and 3)

an earthquake (Wu et al. 2008; Li et al. 2014). This suggests that the estimated swelling pressure represents a minimum value. Thus, the effective stress could be low, with the mechanical behaviour of the fault governed mainly by cohesion rather than the frictional strength before the earthquake. However, the stress state of the fault during the coseismic slip might be influenced by dynamic processes, such as thermal pressurisation (Sibson 1973; Ujiie et al. 2013). Previous high-velocity friction experiments on the JFAST samples revealed that both the peak shear stress and fracture energy decrease as the normal stress decreases (Ujiie et al. 2013), suggesting that earthquake rupture propagates more easily at lower normal stresses. If the effective normal stress state

Kameda *et al. Earth, Planets and Space*   (2019) 71:131

Page 6 of 7

was reduced by the high smectite swelling pressure, this low-barrier state could effectively facilitate slip propagation toward the trench during the earthquake.

Supplementary information

Supplementary information accompanies this paper at https://doi.org/10.1186/s40623-019-1108-5.

Additional file 1. Detailed information on samples, apparatus, and experimental procedures.

Abbreviations
IODP: Integrated Ocean Drilling Program; mbsf: Meters below the sea floor; MAD: Moisture and density; DW: Distilled water.

Authors' contributions
JK, MC, KU, YH and GK designed this study. JK and MU carried out the experiment. MC conducted porosity estimation from the logging data. JK and MC wrote the main manuscript text. JK and MU prepared figures. All authors read and approved the final manuscript.

Availability of data and materials
Data are available on request by contacting JK.

Competing interests
The authors declare that they have no competing interests.

Author details
[1] Department of Earth and Planetary Sciences, Graduate School of Science, Hokkaido University, N10 W8, Sapporo 060-0810, Japan. [2] Graduate School of Environmental Studies, Tohoku University, Aoba 6-6-20, Aramaki Aoba-ku, Sendai 980-8579, Japan. [3] CNRS, GeoRessources Lab, Nancy School of Mines, Universite de Lorraine, Campus ARTEM, 54000 Nancy, France. [4] Graduate School of Life and Environmental Sciences, University of Tsukuba, 1-1-1 Tennodai, Tsukuba 305-0006, Japan. [5] Kochi Institute for Core Sample Research, Japan Agency for Marine-Earth Science and Technology, Nankoku 783-8502, Japan. [6] Tokyo University of Marine Science and Technology, Konan, Minato-ku, Tokyo 108-8477, Japan.

References
Blum P (1997) Physical properties handbook: a guide to the shipboard measurement of physical properties of deep-sea cores. ODP Tech Note. https://doi.org/10.2973/odp.tn.26.1997

Bolt GH (1955) Analysis of the validity of the Gouy-Chapman theory of the electric double layer. J Colloid Sci 10:206–219

Bourlange S, Henry P, Moore JC, Mikada H, Klaus A (2003) Fracture porosity in the decollement zone of Nankai accretionary wedge using logging while drilling resistivity data. Earth Planet Sci Lett 209:103–112

Chatterji PK, Morgenstern NR (1990) A modified shear strength formulation for swelling of clay soils. In: Hoddinott KB, Lamb RO (eds) Physico-chemical aspects of soil and related materials. American Society for Testing and Materials, Philadelphia, pp 118–135

Chester FM, Mori JJ, Toczko S, Eguchi N, the Expedition 343/343T Scientists (2012) Japan trench fast drilling project (JFAST). IODP preliminary report 343/343T. https://doi.org/10.2204/iodp.pr.343343t

Chester FM et al (2013) Structure and composition of the plate-boundary slip zone for the 2011 Tohoku-Oki earthquake. Science 342:1208–1211. https://doi.org/10.1126/science.1243719

Conin M, Henry P, Bourlange S, Raimbourg H, Reuschlé T (2011) Interpretation of porosity and LWD resistivity from the Nankai accretionary wedge in light of clay physicochemical properties: evidence for erosion and local overpressuring. Geochem Geophys Geosyst. https://doi.org/10.1029/2010gc00338

Conin M, Bourlange S, Henry P, Boiselet A, Gaillot P (2014) Distribution of resistive and conductive structures in Nankai accretionary wedge reveals contrasting stress paths. Tectonophysics 611:181–191

Deng X, Underwood MB (2001) Abundance of smectite and the location of a plate boundary fault, Barbados accretionary prism. Geol Soc Am Bull 113:495–507

Fujii Y, Satake K, Sakai S, Shinohara M, Kanazawa T (2011) Tsunami source of the 2011 off the Pacific coast of Tohoku earthquake. Earth Planets Space 63:815–820. https://doi.org/10.5047/eps.2011.06.010

Fujiwara T et al (2011) The 2011 Tohoku-oki earthquake: displacement reaching the trench axis. Science 334:1240. https://doi.org/10.1126/science.1211554

Fulton PM et al (2013) Low coseismic friction on the Tohoku-oki fault determined from temperature measurements. Science 342:1214–1217. https://doi.org/10.1126/science.1243641

Gao X, Wang KL (2014) Strength of stick-slip and creeping subduction megathrusts from heat flow observations. Science 345:1038–1041. https://doi.org/10.1126/science.1255487

Hedin A (2004) Integrated near-field evolution model for a KBS-3 repository: SKB report R-04-36. Swedish Nuclear Fuel and Waste Management Company Limited, Stockholm

Ide S, Baltay A, Beroza GC (2011) Shallow dynamic overshoot and energetic deep rupture in the 2011 Mw 9.0 Tohoku-oki earthquake. Science 332:1426–1429. https://doi.org/10.1126/science.1207020

Ikari MJ, Saffer DM, Marone C (2007) Effect of hydration state on the frictional properties of montmorillonite-based fault gouge. J Geophys Res 112:B06423. https://doi.org/10.1029/2006JB004748

Kameda J, Yamamoto Y, Kimura G (2010) Smectite swelling in the Miura-Boso accretionary prism: possible cause for incipient décollement zone formation. Tectonophysics 494:75–84

Kameda J, Hina S, Kobayashi K, Yamaguchi A, Hamada Y, Yamamoto Y, Hamahashi M, Kimura G (2012) Silica diagenesis and its effect on interplate seismicity in cold subduction zones. Earth Planet Sci Lett 317–318:136–144

Kameda J et al (2015) Pelagic smectite as an important factor in tsunamigenic slip along the Japan Trench. Geology 43:155–158. https://doi.org/10.1130/G35948.1

Kameda J, Inaoi C, Conin M (2016) Exchangeable cation composition of the smectite-rich plate boundary fault at the Japan Trench. Geophys Res Lett. https://doi.org/10.1002/2016GL068283

Kimura G, Hina S, Hamada Y, Kameda J, Tsuji T, Kinoshita M, Yamaguchi A (2012) Runaway slip to the trench due to rupture of highly pressurized megathrust beneath the middle trench slope: the tsunamigenesis of the 2011 Tohoku earthquake off the east coast of northern Japan. Earth Planet Sci Lett 339–340:32–45

Kodaira S et al (2012) Coseismic fault rupture at the trench axis during the 2011 Tohoku-oki earthquake. Nat Geosci 5:646–650. https://doi.org/10.1038/NGEO1547

Komine H, Yasuhara K, Murakami S (2009) Swelling characteristics of bentonites in artificial seawater. Can Geotech J 46:177–189. https://doi.org/10.1139/T08-120

Li HB et al (2014) Structural and physical property characterization in the Wenchuan earthquake fault scientific drilling project—hole 1 (WFSD-1). Tectonophysics 619:86–100

Logan JM, Rauenzahn KA (1987) Frictional dependence of gouge mixtures of quartz and montmorillonite on velocity, composition, and fabric. Tectonophysics 144:87–108

Mitchell JK, Soga K (2005) Fundamentals of soil behavior, 3rd edn. Wiley, New York, pp 111–130

Kameda *et al. Earth, Planets and Space*   (2019) 71:131

Page 7 of 7

Moore DE, Lockner DA (2007) Friction of the smectite clay montmorillonite. In: Dixon T, Moore J (eds) The seismogenic zone of subduction thrust faults. Colombia University Press, New York, pp 317–345

Saffer DM, Frye KM, Marone C, Mair K (2001) Laboratory results indicating complex and potentially unstable frictional behavior of smectite clay. Geophys Res Lett 28:2297–2300

Schleicher AM, Boles A, van der Pluijm BA (2015) Response of natural smectite to seismogenic heating and potential implications for the 2011 Tohoku earthquake in the Japan Trench. Geology 43:755–758. https://doi.org/10.1130/G36846.1

Sibson RH (1973) Interactions between temperature and pore-fluid pressure during earthquake faulting and a mechanism for partial or total stress relief. Nature 243:66–68

Tanaka A, Yamano M, Yano Y, Sasada M (2004) Geothermal gradient and heat flow data in and around Japan (I): appraisal of heat flow geothermal gradient data. Earth Planets Space 56:1191–1194. https://doi.org/10.1186/BF03353339

Tessier D, Dardaine M, Beaumont A, Jaunet AM (1998) Swelling pressure and microstructure of an activated swelling clay with temperature. Clay Miner 33:255–267

Tripathy S, Sridharan A, Schanz T (2004) Swelling pressures of compacted bentonites from diffuse double layer theory. Can Geotech J 41:437–450

Ujiie K et al (2013) Low coseismic shear stress on the Tohoku-Oki megathrust determined from laboratory experiments. Science 342:1211–1214. https://doi.org/10.1126/science.1243485

van Olphen H (1963) An introduction to clay colloid chemistry: for clay technologists. New York, Geologists and Soil Scientists, Interscience Publishers, pp 260–293

Vrolijk P, van der Pluijm BA (1999) Clay gouge. J Struct Geol 21:1039–1048

Wu YH et al (2008) Core-log integration studies in hole-A of Taiwan Chelungpu-fault drilling project. Geophys J Int 174:949–965

Yamano M, Kinoshita M, Goto S (2008) High heat flow anomalies on an old oceanic plate observed seaward of the Japan trench. Int J Earth Sci 97:345–352. https://doi.org/10.1007/s00531-007-0280-1

Publisher's Note